eLIFE elifesciences.org

RESEARCH ARTICLE

Figures and figure supplements

The interplay of stiffness and force anisotropies drives embryo elongation

Thanh Thi Kim Vuong-Brender *et al*

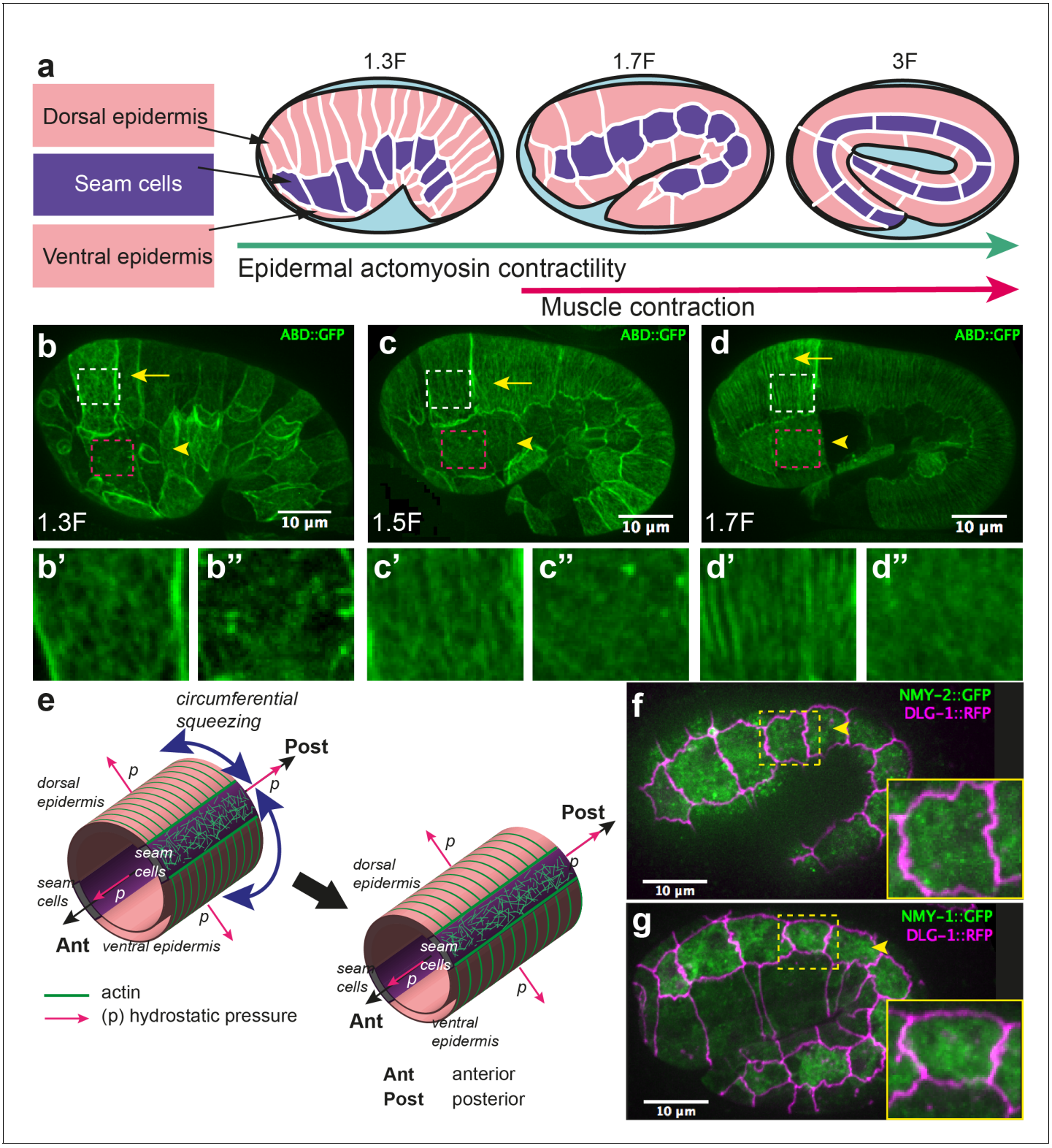

Figure 1. Overview of *C. elegans* embryonic elongation. (**a**) Embryonic elongation in *C. elegans* is driven in part by epidermal actomyosin contractility and in part by muscle contractions. The length of the embryo is used for staging: 2-fold (2F) stage means roughly 2-fold increase in length from the beginning of elongation. Representative stages are shown; anterior to the left, dorsal up. (**b, c, d**) Actin filament organization at the 1.3F, 1.5F and 1.7F stages, respectively, visualized with an ABD::GFP marker. Actin filaments progressively organize into circumferential parallel bundles in DV cells (arrows), arrowheads point to seam cells. Note that the integrated ABD::GFP marker shows some cell to cell variation in expression. (**b', b'', c', c'', d', d''**) Close-

Figure 1 continued on next page

Figure 1 continued

up images of actin pattern in DV cells (from the area in the white rectangle) and seam cells (from the area in the pink rectangle), respectively, of the images in (**b**), (**c**) and (**d**) respectively. (**e**) Actomyosin forces squeeze the embryo circumferentially to make it elongate in the antero-posterior direction. (**f, g**) Endogenous distribution of the two non-muscle myosin II isoforms visualized with the CRISPR GFP-labelled myosin heavy chains NMY-2 (f) and NMY-1 (g). Arrowheads point to seam cells, which are delineated by the junctional marker DLG-1::RFP.

DOI: 10.7554/eLife.23866.003

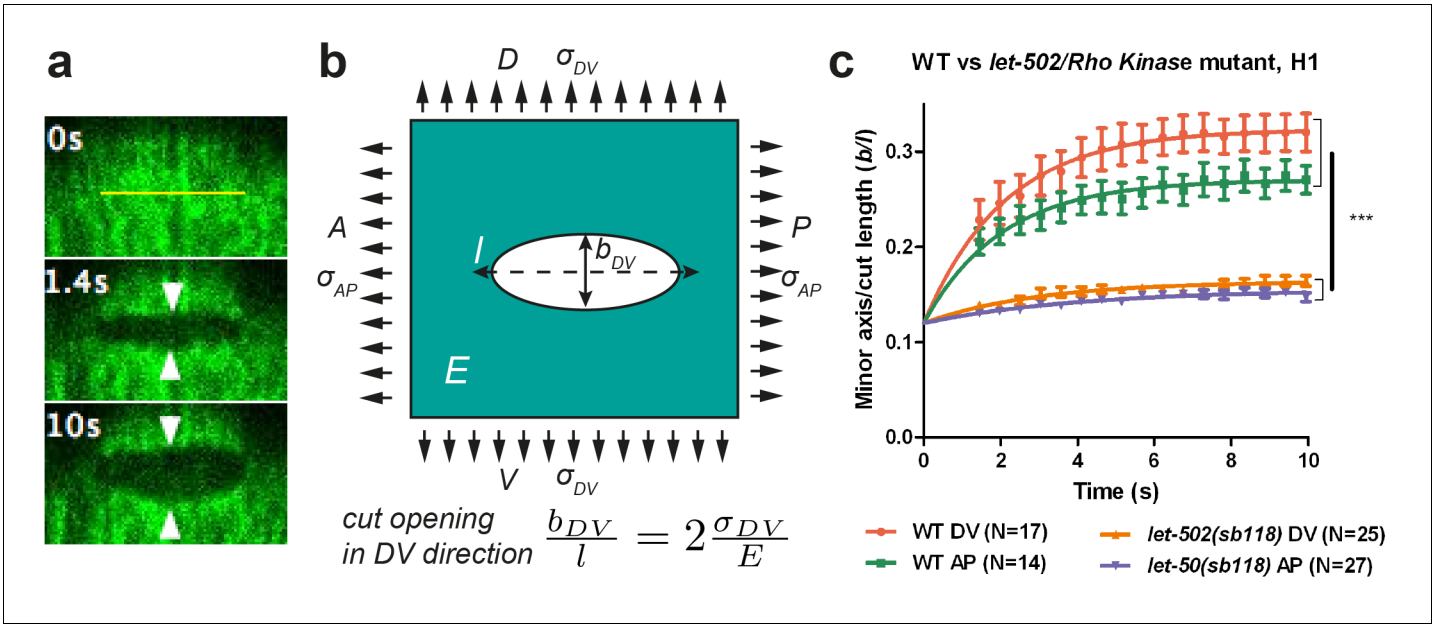

Figure 2. Physical model using the shape of the cut opening at equilibrium to measure the ratio of stress to Young modulus. (**a**) The GFP-labelled actin cortex of HYP7 dorsal epidermal cell at the 1.7F stage before (0 s), 1.4 s and 10 s after laser severing; the cut made along the AP direction and was 5 µm in length. Double arrowheads indicate the distance between cut borders, which increases with time. (**b**) Model of epidermal cells as an infinite elastic plane under biaxial stress in the AP and DV directions after an incision of length *l*. The final shape of the cut opening is an ellipse. The cut opening in the DV direction (after an incision along the AP direction) depends on the stress along the DV direction and the Young modulus (see text). (**c**) The opening depends on myosin II activity: comparison of the cut response in the seam cell H1 between wild-type (WT) and *let-502(sb118)/Rho kinase* mutant embryos at a stage when muscles start to twitch (around 1.5F). The average value and standard error are reported. Time zero, moment of the cut; DV and AP show direction of opening. Two-tailed t-test, ***p=$4*10^{-7}$ between WT DV and *let-502(sb118)* DV, p=$4*10^{-6}$ between WT AP and *let-502(sb118)* AP; N, number of embryos examined.

DOI: 10.7554/eLife.23866.004

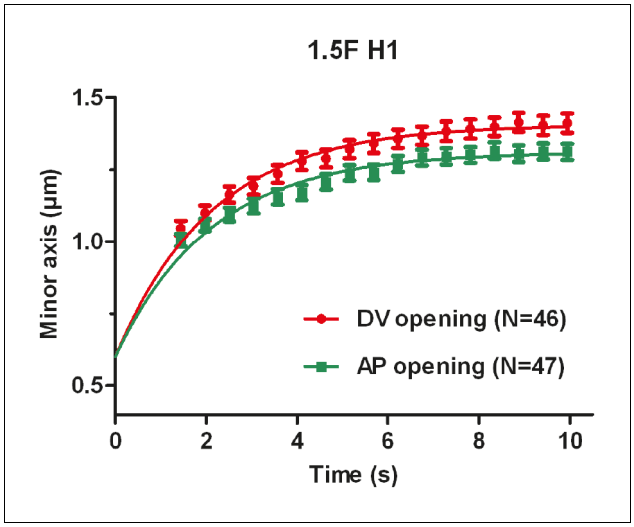

Figure 2—figure supplement 1. Evolution of the distance between the cut borders (the minor axis of the cut opening) versus time. The average value and standard error are reported. Time 0 is the moment of the cut. Solid lines show the single exponential fit with an initial width of cut opening of 0.6 µm (see Materials and methods).
DOI: 10.7554/eLife.23866.005

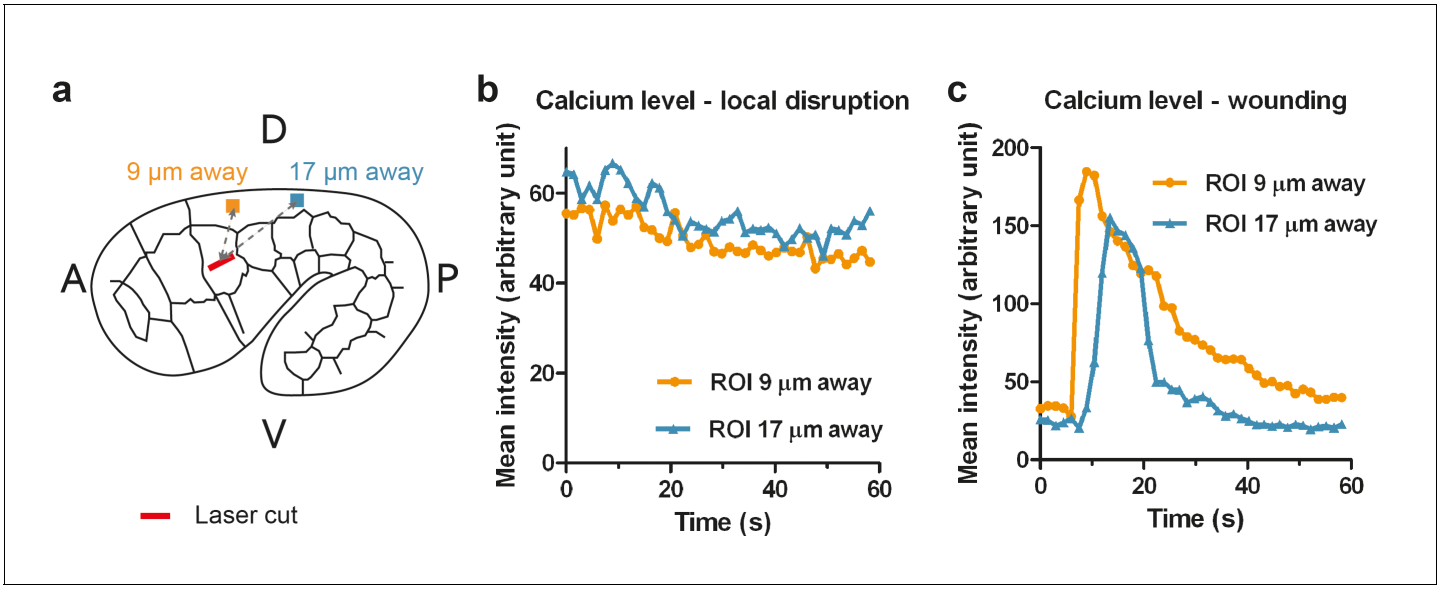

Figure 2—figure supplement 2. Calcium imaging of ablated embryos. (**a**) Scheme for measuring the calcium sensor GCaMP3 mean fluorescence intensity at positions 9 µm and 17 µm away from the cut site (red bar). The intensity was averaged over a region of interest (ROI) of 1.5 × 1.5 μm^2. A, anterior; P, posterior; D, dorsal; V, ventral. (**b, c**) Calcium level over time for an embryo typical of the majority of ablated embryos, in which the cortex is probably disrupted locally (**b**), or of the minority of ablated embryos, in which the wounding response is probably more severe (**c**).
DOI: 10.7554/eLife.23866.006

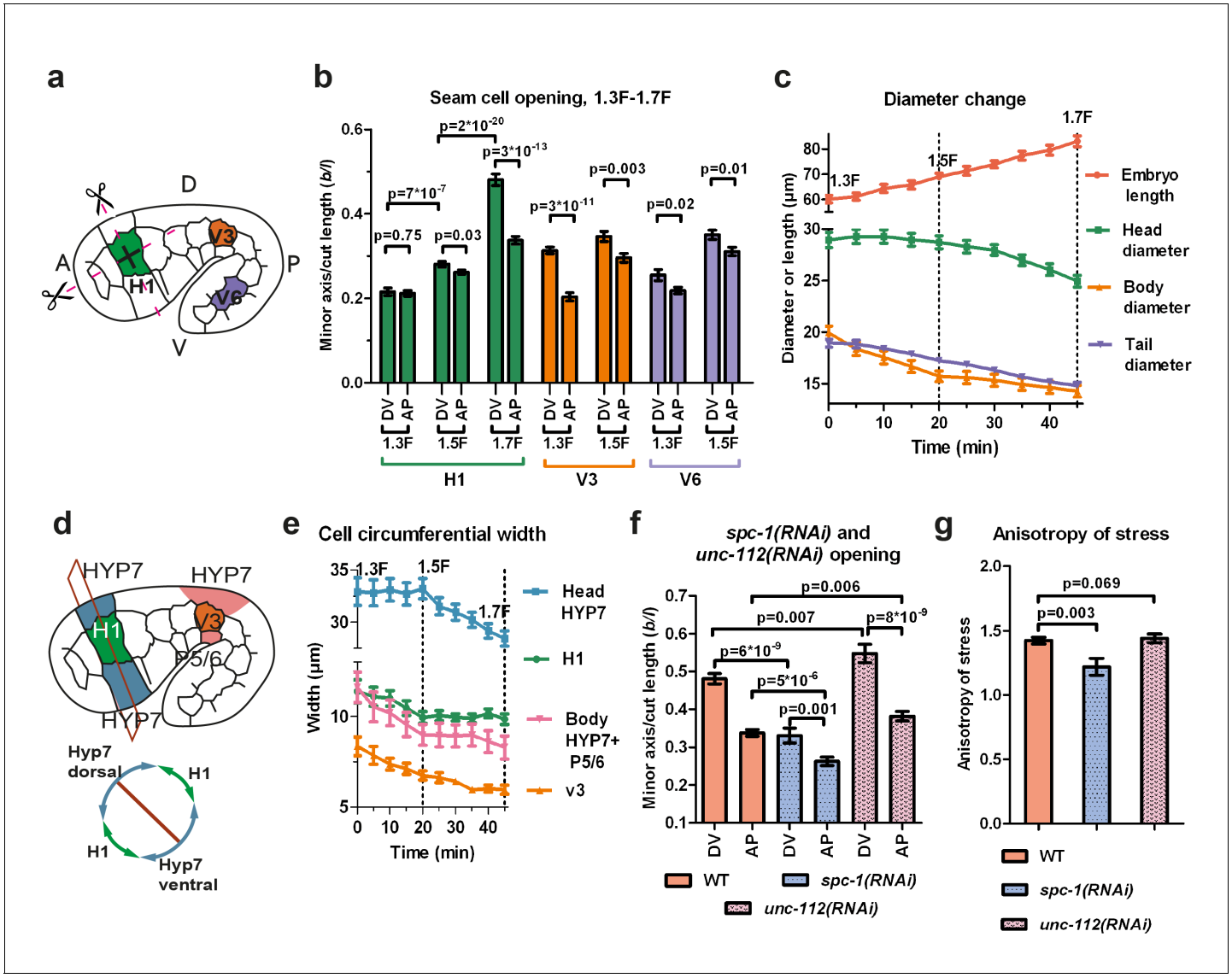

Figure 3. Stress anisotropy in seam cells correlates with morphological changes and partially depends on the spectrin cytoskeleton. (**a**) Scheme showing laser ablation experiments in the AP and DV directions for H1, V3 and V6 seam cells at different stages. A, anterior; P, posterior; D, dorsal; V, ventral. (**b**) Cut opening in H1, V3 and V6 from the 1.3F to the 1.7F stages (see ***Figure 2b***). The p-values from two-tailed t-tests are reported. (**c**) Changes in embryo length, head diameter at the level of H1, body diameter at the level of V3 and tail diameter at the level of V6, between the 1.3F and 1.7F stages. N = 10. (**d**) Scheme showing the measurement of circumferential cell width in the head (above) and corresponding section (below). (**e**) The circumferential width of H1, V3, head and body DV cells (averaged for dorsal and ventral cells). N = 10. (**f**) Measures of the cut opening in H1 for WT, *spc-1(RNAi)* treated and *unc-112(RNAi)* muscle-defective embryos at a stage equivalent to the 1.7F stage. The p-values of two-tailed t-tests are reported. (**g**) Comparison of the stress anisotropy in H1, defined by DV/AP stress, between WT 1.7F stage, *spc-1(RNAi)* embryos and *unc-112(RNAi)* embryos at the equivalent 1.7F stage. The p-values of Z-tests are reported. The number of embryos used for ablation is given in ***Supplementary file 1***. For (**b**,**c**,**e**–**g**), the average (or calculated) values and standard errors are reported.

DOI: 10.7554/eLife.23866.011

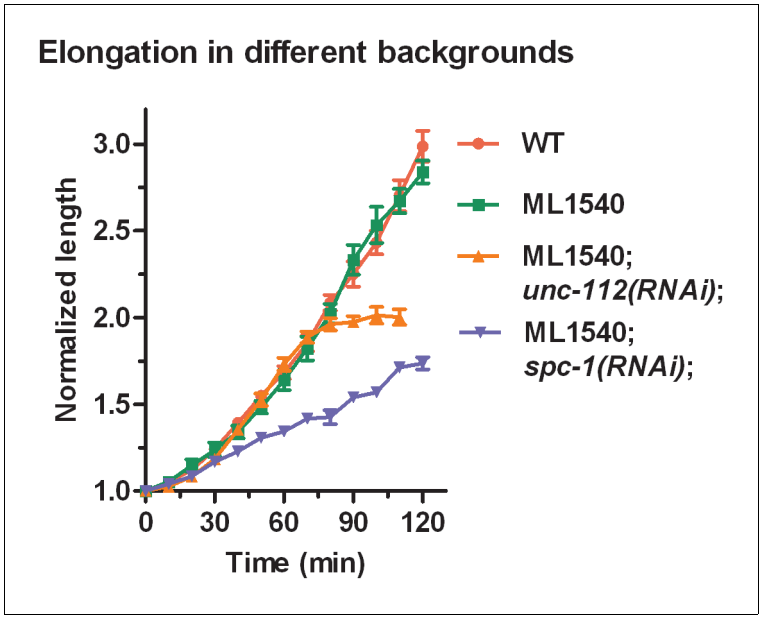

Figure 3—figure supplement 1. Elongation curves normalized to the initial embryo length for different genetic backgrounds. ML1540 is the strain carrying the actin-binding domain fused to GFP (see Materials and methods). The average value and standard error are reported. N ≥ 9 for each genotype.
DOI: 10.7554/eLife.23866.012

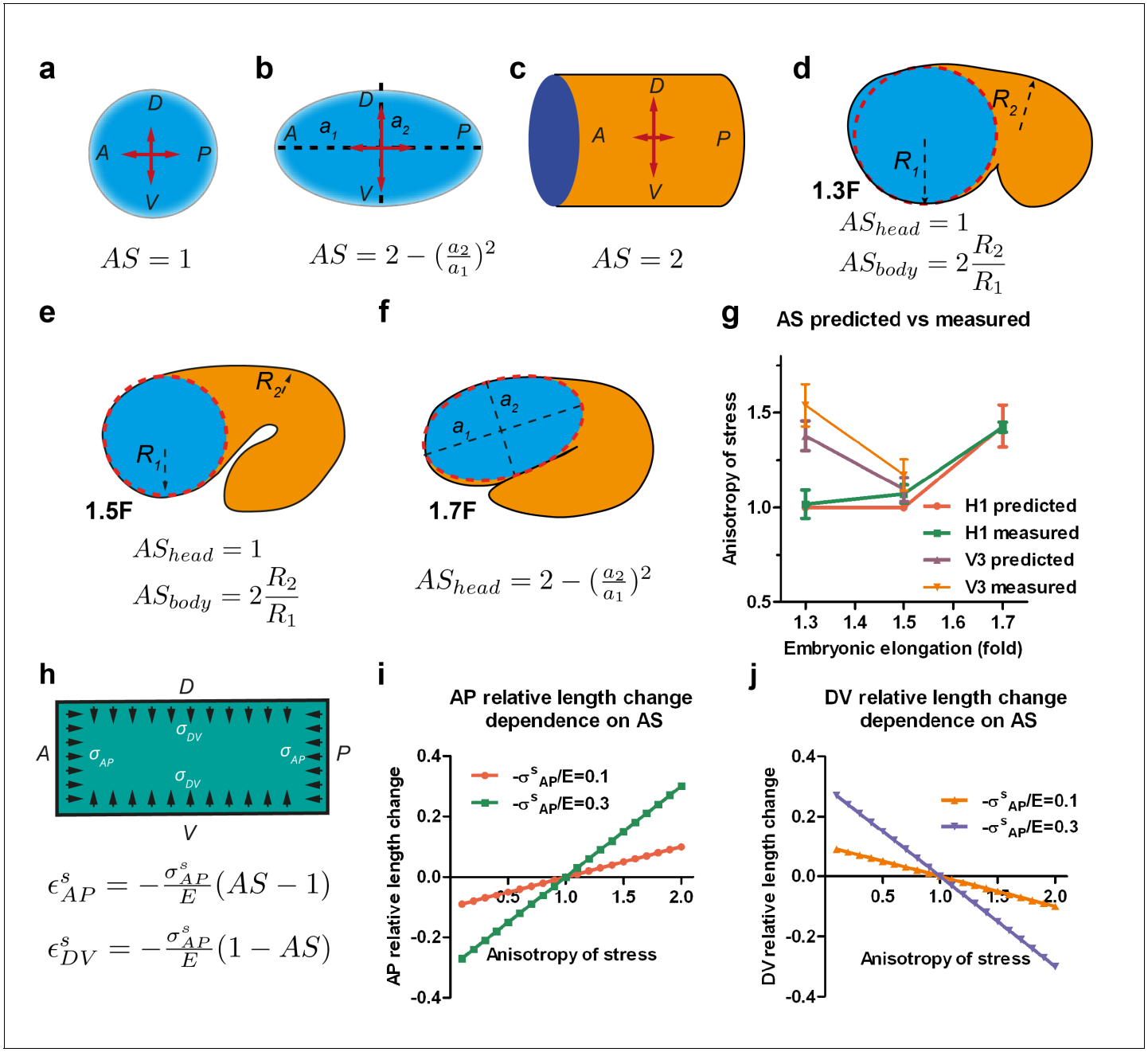

Figure 4. Stress anisotropy induces embryonic morphological changes. (**a, b, c**) Anisotropy of stress (AS) for a sphere (a), an ellipsoid (b) and a cylinder (c) with DV and AP axis defined in the schemes; (**a, b**) show the middle plane; the major and minor axis of the ellipsoid are called a_1 and a_2. (**d, e, f**) The embryo is schematized with a spherical (1.3F and 1.5F stages) or ellipsoidal (1.7F stage) head, and a curved cylindrical body. The AS in the head evolves from 1 (sphere) to that of an ellipsoid, whereas the body AS depends on the ratio of body to head radius (R_2/R_1). (**g**) Comparison of the predicted AS based on embryo diameter measurements (see ***Figure 3c***) and the measured AS obtained from laser ablation experiments (***Figure 3b***). (**h**) Hooke's law written for an isotropic material like seam cells (Appendix 6A); ϵ^s_{AP} and ϵ^s_{DV} are the relative length changes along the AP and DV directions, respectively. The stress σ^s_{AP} and σ^s_{DV} along the AP and DV directions are supposed to be contractile (so negative). *E*, seam cell Young modulus; A, anterior; P, posterior; D, dorsal; V, ventral. (**i, j**) Dependence of the AP and DV relative length change on the AS for different values of σ^s_{AP}/E.

DOI: 10.7554/eLife.23866.013

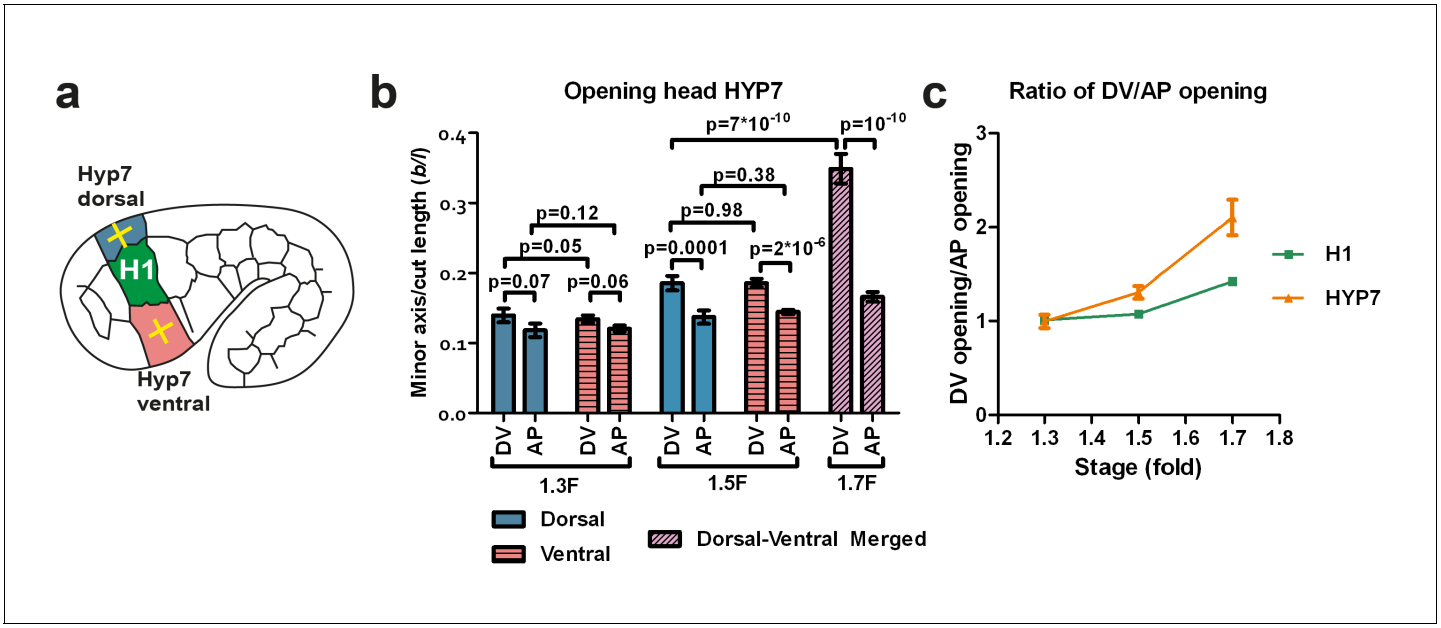

Figure 5. The dorso-ventral epidermis behaves differently than the H1 seam cell in ablation experiments. (**a**) Scheme showing laser ablation experiments in the epithelial cell HYP7 dorsal and ventral to H1, yellow crosses show cut directions. (**b**) Cut opening in the DV and AP directions measured in HYP7 between the 1.3F and 1.7F stages (see ***Figure 2b***). p-values of two-tailed t-tests are reported. (**c**) Comparison of the DV/AP opening ratio in the seam cell H1 and in the head HYP7 cell. The data were derived from Figures 3b and 5b. To simplify, we will call the cells that will form the future HYP7 syncytium the HYP7 cells. The average (or computed) values and standard errors are reported. The numbers of embryos used for ablation are given in ***Supplementary file 1***.

DOI: 10.7554/eLife.23866.014

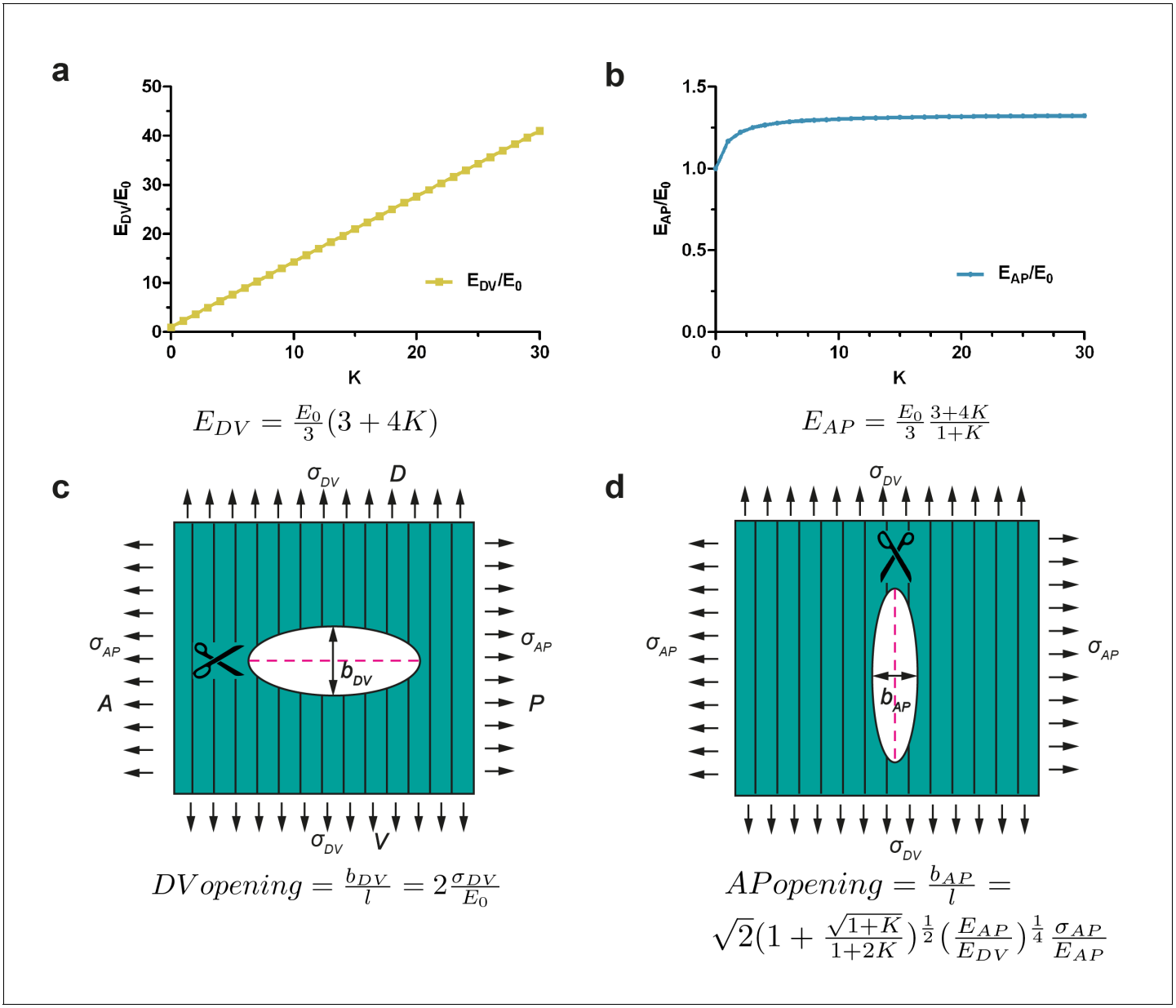

Figure 6. Model of cut opening for a fiber-reinforced material. (**a**) Considering a composite material with fiber reinforcement along the DV direction, the ratio of the Young modulus of the composite material along the DV direction, E_{DV}, to the Young modulus of the material without fibers (matrix), E_0, depends linearly on a factor K (see Appendix 7); K is related to fiber density and stiffness. (**b**) The ratio of the Young modulus along the AP direction, E_{AP}, to the matrix Young modulus, E_0, varies little with K. (**c**) The opening of the cuts perpendicular to the fibers is similar to an isotropic plane response, and depends on the ratio of DV stress to the matrix Young modulus σ_{DV}/E_0. (**d**) The opening of the cuts parallel to the fibers depends on the factor K, the ratio of AP/DV stiffness, E_{AP}/E_{DV}, and the ratio of stress over Young modulus in the AP direction, σ_{AP}/E_{AP}.

DOI: 10.7554/eLife.23866.015

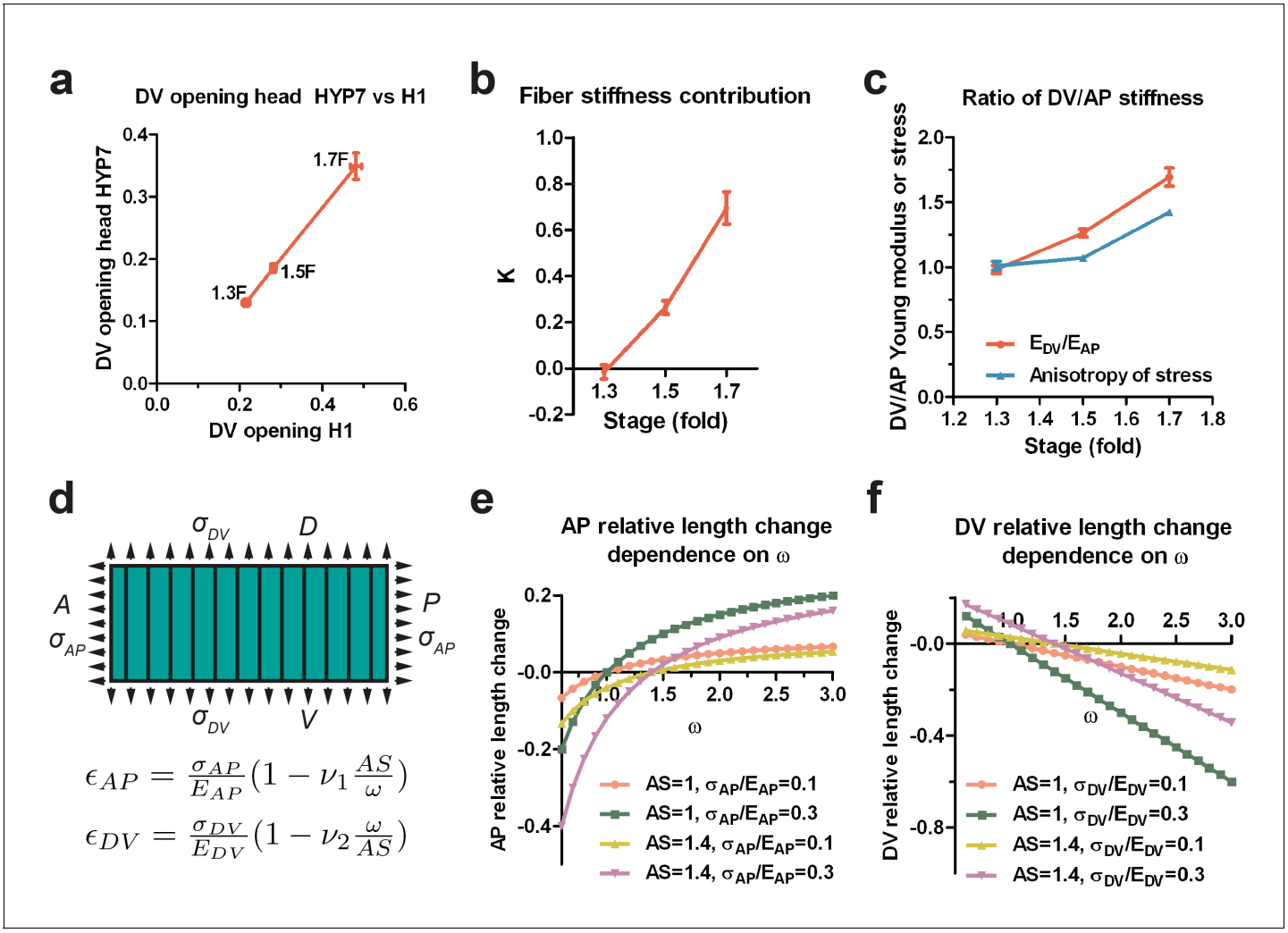

Figure 7. The anisotropy of stiffness in the HYP7 cell helps the embryo to elongate. (**a**) The cut opening in HYP7 is linearly related to the cut opening in H1. The slope of the linear regression gives the ratio of the HYP7 matrix without fibers to H1 Young moduli. (**b**) The factor *K* increases during elongation from the 1.3F to 1.7F stages. (**c**) The ratio of DV/AP stiffness increases and is greater than the AS during early elongation. The data were derived from ***Figure 3c*** and Appendix 10. (**d**) Hooke's law written for a fiber-reinforced material such as DV cells (Appendix 6B). ϵ_{AP} and ϵ_{DV} are the relative length change along the AP and DV directions, respectively. The stresses σ_{AP} and σ_{DV} along the AP and DV directions, respectively are supposed to be tensile (so positive). E_{AP} and E_{DV} are the Young moduli in the DV cells along the AP and DV direction, respectively. ν_1 and ν_2 are Poisson's ratios in DV cells; ω is the E_{DV}/E_{AP} ratio. A, anterior; P, posterior; D, dorsal; V, ventral. (**e**) Dependence of the AP relative length change ϵ_{AP} on the ratio of DV/AP stiffness ω for different values of AS and σ_{AP}/E_{AP}; the ν_1 value is taken to be 1. (**f**) Dependence of the DV relative length change ϵ_{DV} on the ratio of DV/AP stiffness ω for different values of *AS* and σ_{DV}/E_{DV}; the ν_2 value is taken to be 1. For (**a–c**), the average (or computed) values and standard errors are reported.

DOI: 10.7554/eLife.23866.016

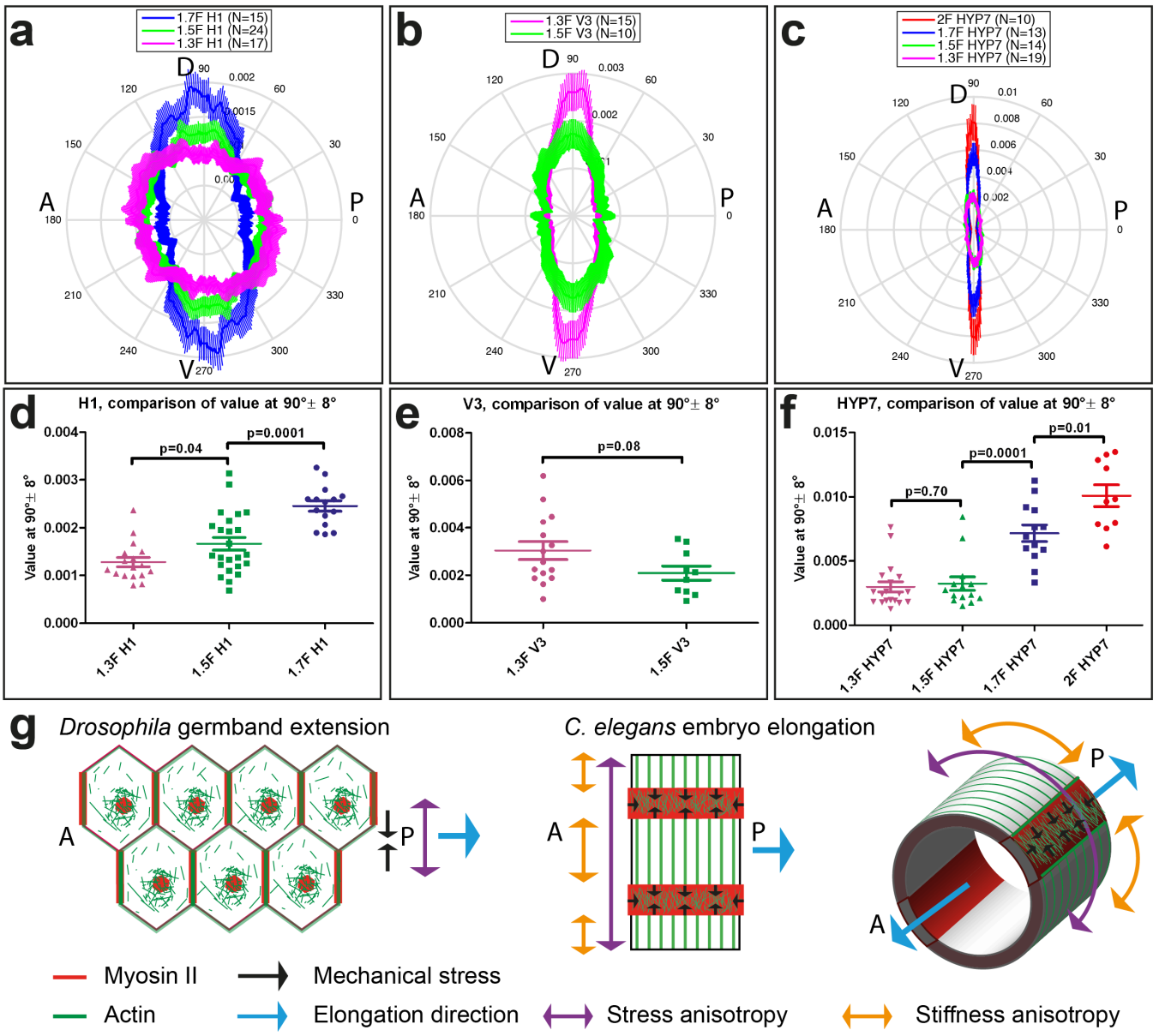

Figure 8. Actin filament organization correlated with stress and stiffness anisotropy pattern. (**a–c**) Angle distribution of actin filaments in the seam cell H1 (**a**), seam V3 (**b**) and the HYP7 cell (**c**), at different elongation stages. D, dorsal; V, ventral; A, anterior; P, posterior. 90° correspond to DV direction. (**d, e, f**) Comparison of the peak values at 90° ± 8° (DV direction) of angular distribution showed in (**a, b, c**), respectively. p-values of two-tailed t-tests are reported. (**g**) (Left) The anisotropy of mechanical stress generated by the polarized actomyosin network and medial myosin pulses promote *Drosophila* germband extension. (Right) The interplay of stress anisotropy (generated in seam cells - red) and stiffness anisotropy (DV cells – white) promote *C. elegans* embryo elongation. Note that, although myosin II does not display a polarized distribution within individual *C. elegans* epidermal cells as it does in *Drosophila* germband epithelial cells, its enrichment in seam cells along the circumference is reminiscent of the localized myosin II enrichment at vertical junctions in *Drosophila*. A, anterior; P, posterior. For (**a–f**), the average values and standard errors are reported.

DOI: 10.7554/eLife.23866.017

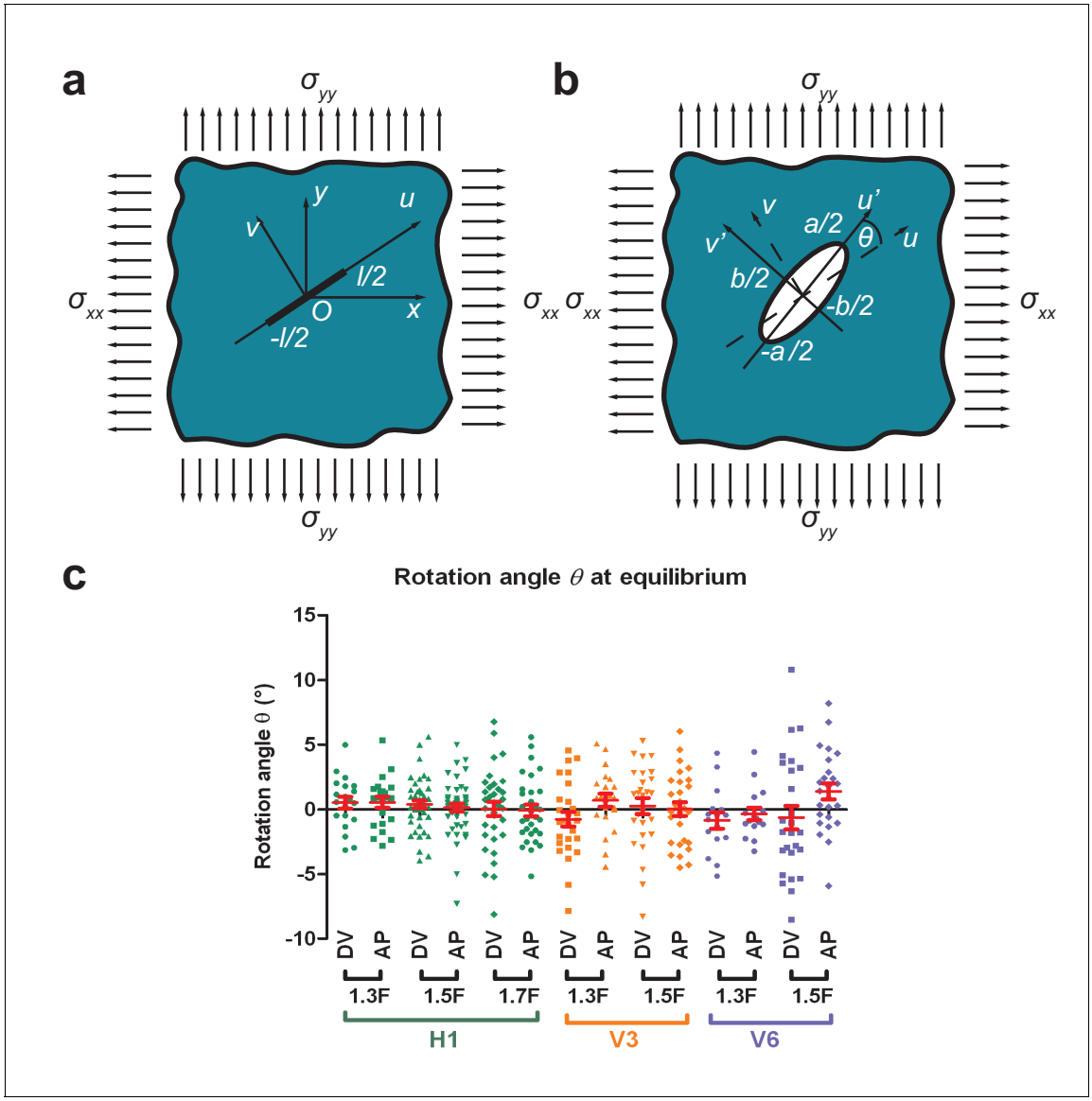

Appendix 2—figure 1. Determination of stress loading directions from cut shape rotation. (**a**) An incision of length l was introduced in an elastic plane under biaxial stress along the x and y directions. The cut was along the u axis with the uv coordinates. (**b**) The shape of the opening at equilibrium was an ellipse (***Theocaris et al., 1986***). We called u' (of $u'v'$ coordinates) the axis parallel to the major axis of the opening ellipse, which formed an angle θ to the direction of the initial cut. (**c**) The rotation angle θ at equilibrium (measured around 9.5 s after cut) for H1 from the 1.3F to the 1.7F stages and for V3 and V6 from the 1.3F to the 1.5F stages. 'DV' and 'AP' mean DV and AP opening, respectively. Red bars show the means and standard errors.
DOI: 10.7554/eLife.23866.021

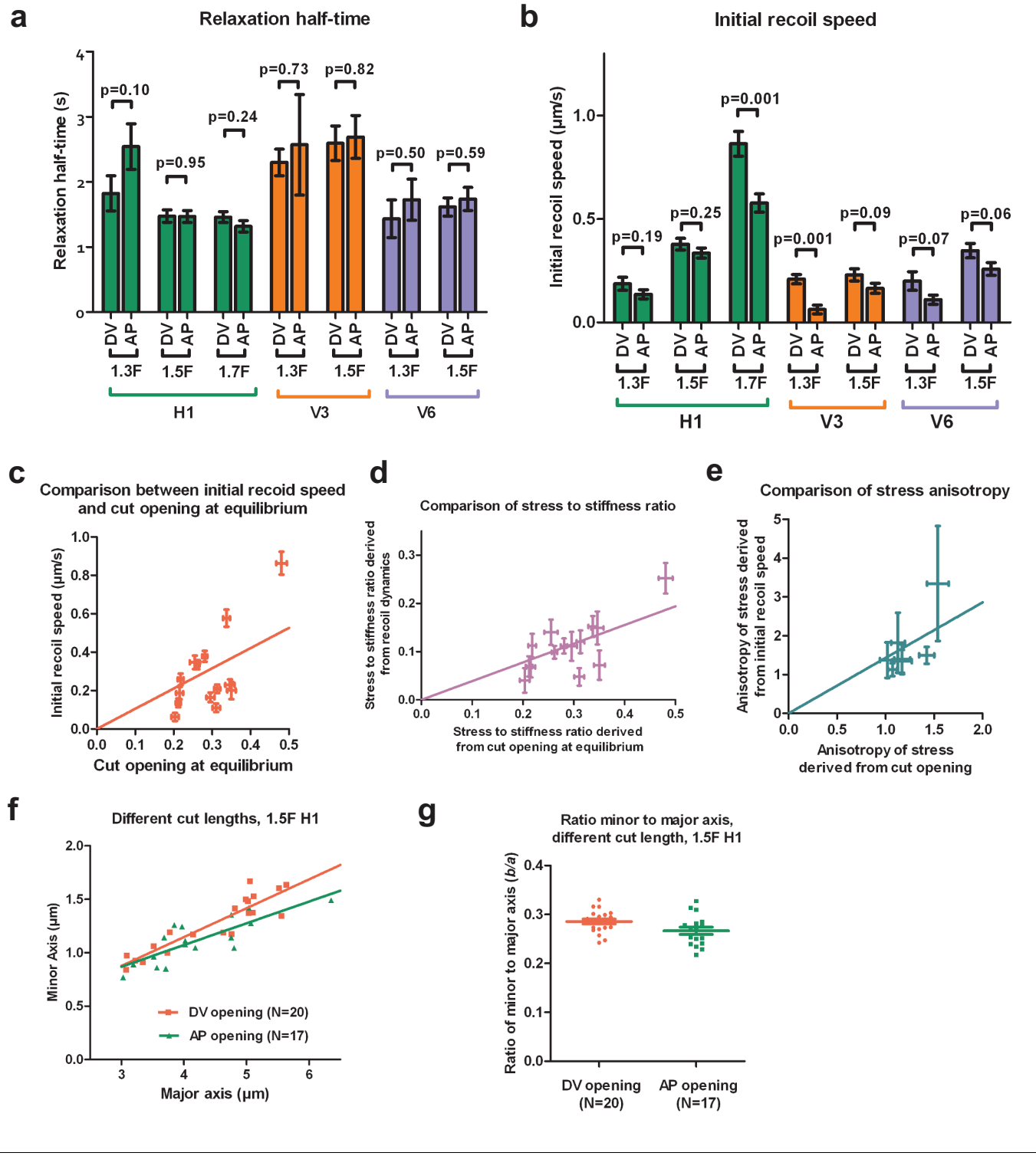

Appendix 3—figure 1. Comparison of stress and material properties derived from ablation cut recoil dynamics and opening shape. (**a**) Relaxation half-time and (**b**) initial recoil speed derived from fitting the cut border relaxation using an initial width of cut opening of 0.6 μm, in H1, V3 and V6 from the 1.3F to the 1.7F stages. Z-test, ns, $p>0.05$; **$0.001<p<0.01$; ***$p<0.001$. DV and AP indicate the directions of opening. (**c**) Comparison between the ratio of stress to stiffness derived using the cut recoil dynamics (after normalization to the cut length) and that derived from the cut opening at equilibrium. (**d**) Comparison of stress to stiffness ratio measured from the recoil dynamics versus that derived using cut opening at equilibrium. (**e**) Comparison of

Appendix 3—figure 1 continued on next page

Appendix 3—figure 1 continued

the anisotropy of stress (defined by DV/AP stress) derived from the recoil dynamics and that from the cut opening at equilibrium. (**f**) The minor and major axes of cut opening at equilibrium show a linear relationship when the cut length varied from 3 μm to 6 μm. The ablations were performed in H1 at the 1.5F stage. Solid lines show a linear fit. $R^2 > 0.65$. (**g**) The ratio of the minor to major axis of the cut opening at equilibrium calculated from data shown in (**f**).

DOI: 10.7554/eLife.23866.022

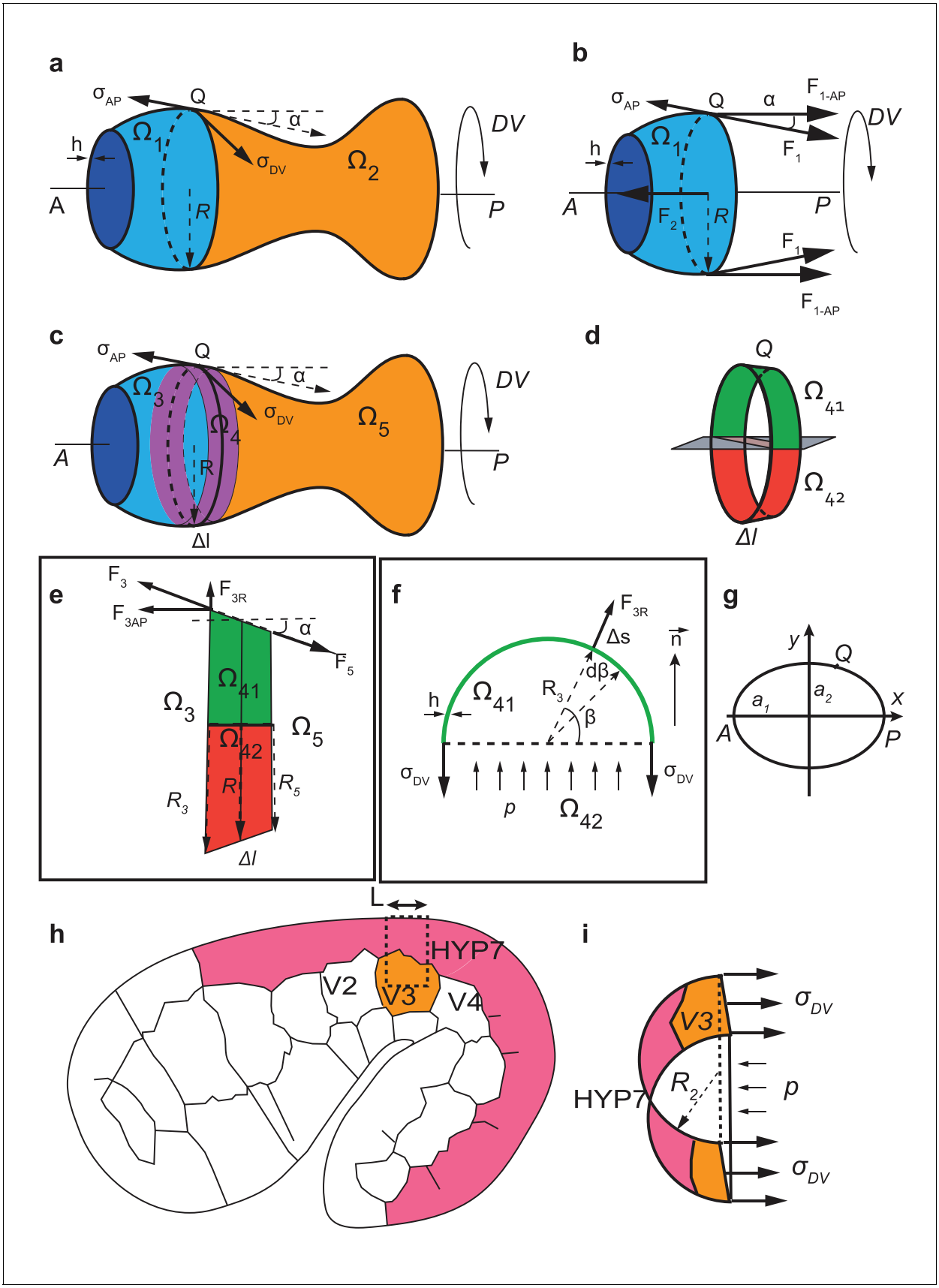
a
σAP
Q
α
h
Ω1
σDV
Ω2
DV
A
R
P
b
σAP
Q
α
F1-AP
h
Ω1
F1
DV
A
F2
R
P
F1
F1-AP
c
σAP
Q
α
Ω3
σDV
Ω5
DV
Ω4
A
R
P
Δl
d
Q
Ω41
Ω42
Δl
e
F3
F3R
F3AP
α
F5
Ω41
Ω3
Ω5
Ω42
R
R5
R3
Δl
f
F3R
Δs
n
dβ
h
Ω41
R3
β
σDV
σDV
p
Ω42
g
y
Q
a1
a2
x
A
P
L
h
HYP7
V2
V3
V4
i
σDV
V3
R2
p
HYP7
σDV

Appendix 5—figure 1. Calculation of anisotropy of stress for an axisymmetric thin-walled pressured vessel and for *C. elegans* embryos at the seam cell V3 position. (**a-f**) Anisotropy of stress for an axisymmetric thin-wall pressured vessel is derived from the force equilibrium equations of a volume element. (**g**) Geometrical configuration for determining anisotropy of stress for an ellipsoide. (**h-i**) The anisoropy of stress at the level of the seam cell V3 is derived from equilibrium equations of a volume element at V3 postition.
DOI: 10.7554/eLife.23866.023

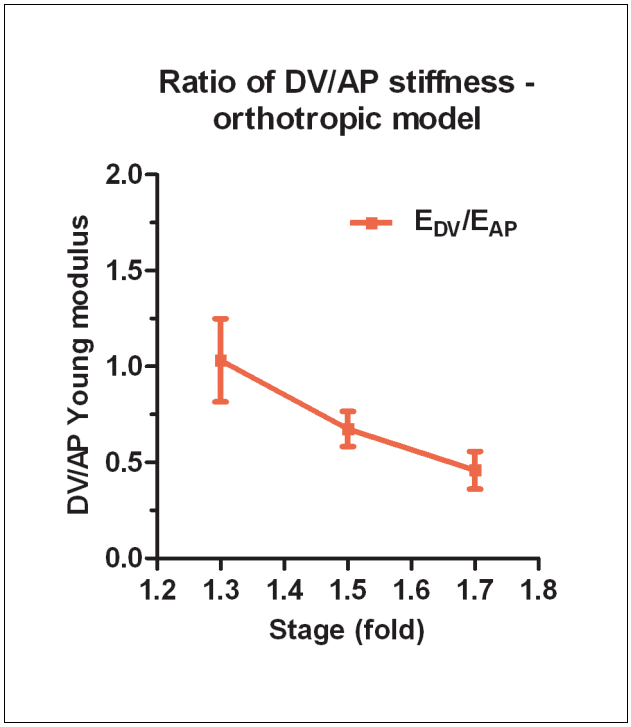

Appendix 8—figure 1. Ratio of DV/AP Young moduli calculated from the orthotropic model for the DV epidermis.
DOI: 10.7554/eLife.23866.024